



---

1    **Evaporation measurement and modelling of an alpine saline lake influenced by freeze–thaw on the**  
2    **Qinghai–Tibet Plateau**

3    Fangzhong Shi<sup>1,2</sup>, Xiaoyan Li<sup>1,2,3,4</sup>, Shaojie Zhao<sup>1,2</sup>, Yujun Ma<sup>5</sup>, Junqi Wei<sup>1,2</sup>, Qiwen Liao<sup>1,2</sup>, Deliang  
4    Chen<sup>6</sup>

5    <sup>1</sup>State Key Laboratory of Earth Surface Processes and Resource Ecology, Faculty of Geographical  
6    Science, Beijing Normal University, Beijing 100875, China;

7    <sup>2</sup>School of Natural Resources, Faculty of Geographical Science, Beijing Normal University, Beijing  
8    100875, China

9    <sup>3</sup>Key Laboratory of Tibetan Plateau Land Surface Processes and Ecological Conservation, Ministry of  
10    Education, Qinghai Normal University, Xining, China

11    <sup>4</sup>Academy of Plateau Science and Sustainability, Qinghai Normal University, Xining, China

12    <sup>5</sup>School of Geography and Planning, Sun Yat–sen University, Guangzhou, China

13    <sup>6</sup>Regional Climate Group, Department of Earth Sciences, University of Gothenburg, Gothenburg,  
14    Sweden.

15    \* To whom the correspondence should be addressed: Xiao–Yan Li, State Key Laboratory of Earth  
16    Surface Processes and Resource Ecology, Beijing Normal University, Beijing, China. Emails:  
17    xyli@bnu.edu.cn.

18    ✉ Fangzhong Shi (during review)    fzshi@mail.bnu.edu.cn

19    ✉ Xiaoyan Li\* (after acceptance)    xyli@bnu.edu.cn

20

21



---

22

23 **Key Points**

- 24 ● Night evaporation of Qinghai Lake accounts for more than 40% of the daily evaporation during  
25 both the ice-free and ice-covered periods.
- 26 ● Lake ice sublimation reaches  $175.22 \pm 45.98$  mm, accounting for 23% of the annual evaporation.
- 27 ● Wind speed weakening may have resulted in an 11.14% decrease in lake evaporation during  
28 the ice-covered period from 2003 to 2017.



---

29 **Abstract**

30 Saline lakes on the Qinghai–Tibet Plateau (QTP) profoundly affect the regional climate and water cycle  
31 through loss of water (E, evaporation under ice–free (IF) and sublimation under ice–covered (IC)  
32 conditions). Due to the observation difficulty over lakes, E and its underlying driving forces are seldom  
33 studied targeting saline lakes on the QTP, particularly during the IC. In this study, E of Qinghai Lake  
34 (QHL) and its influencing factors during the IF and IC were first quantified based on six years of  
35 observations. Subsequently, two models were chosen and applied in simulating E and its response to  
36 climate variation during the IF and IC from 2003 to 2017. The annual E sum of QHL is  $768.58 \pm 28.73$   
37 mm, and E sum during the IC reaches  $175.22 \pm 45.98$  mm, accounting for 23% of the annual E sum. The  
38 E is mainly controlled by the wind speed, vapor pressure difference, and air pressure during the IF, but  
39 driven by the net radiation, the difference between the air and lake surface temperatures, wind speed, and  
40 ice coverage during the IC. The mass transfer model simulates lake E well during the IF, and the model  
41 based on energy achieves a good simulation during the IC. Moreover, wind speed weakening results in  
42 an 11.14% decrease in E during the IC of 2003–2017. Our results highlight the importance of E in IC,  
43 provide new insights into saline lake E in alpine regions, and can be used as a reference to further improve  
44 hydrological models of alpine lakes.

45 **Keywords:**

46 Lake evaporation and sublimation, saline lakes, flux observation, ice–covered period, Qinghai Lake,  
47 Qinghai–Tibet Plateau



---

## 48 1. Introduction

49 Saline lakes account for 23% of the total area and 44% of the total water volume of Earth's lakes  
50 (Wurtsbaugh et al., 2017). They play an important role in shaping the regional climate and maintaining  
51 ecological security and sustainable development in arid regions (Messenger et al., 2016; Wurtsbaugh et  
52 al., 2017; Woolway et al., 2020; Wu et al., 2021; Wu et al., 2022). Under the influences of climate change  
53 and human activities, saline lakes worldwide have changed rapidly in terms of their area, level,  
54 temperature, ice phenology, energy and water exchange, which has become an issue of concern (Gross,  
55 2017; Wurtsbaugh et al., 2017; Woolway et al., 2020). Evaporation under ice-free (IF) and sublimation  
56 under ice-covered (IC) periods (E) is an important mechanism of transfer of energy and water between  
57 lakes and atmosphere, and is one of the main factors influencing changes in the lake water volume (Lazhu  
58 et al., 2016; Ma et al., 2016; Woolway et al., 2018; Guo et al., 2019; Woolway et al., 2020).

59 In contrast to freshwater lakes, E of saline lakes involves a more complex process and is affected not  
60 only by climate conditions but also by the salinity, lake depth, temperature, stratification, thermal stability,  
61 and hydrodynamics (Hamdani et al., 2018). For example, dissolved salt ions can reduce the free energy  
62 of water molecules (i.e., reduced water activity) and result in a reduced saturated vapor pressure above  
63 saline lakes at a given water temperature (Salhotra et al., 1987; Mor et al., 2018). Previous studies have  
64 investigated the relationship between E and salinity of saline lakes and discrepancies in the controlling  
65 factors between different time scales (Salhotra et al., 1987; Lensky et al., 2018; Hamdani et al., 2018;  
66 Mor et al., 2018). These studies have mainly focused on saline lakes in arid and temperate zones, and the  
67 interaction and mutual feedback between the water body of saline lakes and the atmosphere remain  
68 unclear. In particular, there are few studies on E of alpine saline lakes which exhibit complex hydrology  
69 and limnology.

70 Saline lakes account for over 70% of the total lake area on the Qinghai-Tibet Plateau (QTP) (Liu et al.,  
71 2021), and thus profoundly affect the regional climate and water cycle through E (Yang et al., 2021).  
72 However, continuous year-round direct measurements of saline lake E are scarce, which hinders the  
73 exploration of lake E at different time scales. Observations of E from saline lakes have been obtained for  
74 Qinghai Lake (QHL) (Li et al., 2016), Namco (Wang et al., 2015; Ma et al., 2016), Selinco (Guo et al.,  
75 2016), and Erhai (Liu et al., 2015) via the eddy-covariance (EC) technique or pan E on the QTP, but



---

76 these observations are mainly for the growing seasons (or IF: approximately mid–May to mid–October).  
77 Thus, there are considerably fewer E observations during the IC and full–year period of lakes, mainly  
78 because of the harsh environment and limited accessibility to the QTP (Lazhu et al., 2016). However,  
79 most lakes on the QTP exhibit a long and stable IC lasting more than 100 days due to the low annual air  
80 temperature ( $T_a$ ) (Cai et al., 2019), which suggests that E observations are currently lacking for nearly a  
81 quarter of the year (from the IF to the IC). Although studies have commented on the importance of E  
82 during the IC (Li et al., 2016; Wang et al., 2020) and clarified that freezing/breakup processes could result  
83 in sudden changes in lake surface properties (such as albedo and roughness) and affect the water and  
84 energy exchange between the lake and atmosphere (Cai et al., 2019; Yang et al., 2021), the dynamic  
85 processes of energy interchange and E of saline lakes during the IC and its responses to climate warming  
86 on the QTP still constitute a knowledge gap in lake hydrology research. Thus, there is an urgent need to  
87 better quantify lake E during the IC on the QTP.

88 A large number of models have been employed to calculate lake E, mainly including the Dalton formula  
89 series based on mass transfer and aerodynamics, energy and water balance formula series, Penman  
90 formula series considering both aerodynamics and energy balance, and empirical formula based on  
91 statistical analysis (Dalton, 1802; Bowen, 1926; Penman, 1948; Harbeck et al., 1958; Finch and Calver,  
92 2008; Hamdani et al., 2018; Wang et al., 2019a). However, the reported values exhibit large discrepancies  
93 in their seasonal variations and annual amounts between those models (Lazhu et al., 2016; Ma et al.,  
94 2016; Guo et al., 2019; Wang et al., 2019a; Wang et al., 2020), and almost all models were calibrated  
95 and verified against E observations during the IF as a result of the deficiency in observed E during the  
96 IC (Lazhu et al., 2016; Guo et al., 2019), and E during the IC was either not calculated or unverified  
97 (Wang et al., 2020). In addition, compared with small lakes, large and deep lakes exhibit higher E levels  
98 and delayed seasonal E peaks because more energy is absorbed and stored in large and deep lakes during  
99 the IF and released during the IC (Wang et al., 2019a). Thus, the effect of changes in ice phenology on  
100 lake E is particularly important, which calls for different models for E simulation during the IF and IC.

101 Furthermore, with increasing overall surface air warming and moistening, solar dimming, and wind  
102 stilling since the beginning of the 1980s (Yang et al., 2014), lakes on the QTP have experienced a  
103 significant temperature increase (at a rate of  $0.037^\circ\text{C}/\text{yr}$  from 2001 to 2015) (Wan et al., 2018) and ice



---

104 phenology shortening (at a rate of  $-0.73$  d/yr from 2001 to 2017) (Cai et al., 2019). Changes in the air  
105  $T_a$ , water surface temperature ( $T_s$ ), wind speed (WS), and ice phenology could impose different effects  
106 on energy interchange and molecular diffusion due to differences in the state phase and reflectance of  
107 water between the IC and IF, thus altering lake E (Wang et al., 2018). Although many studies have  
108 reported a decrease in E of lakes on the QTP by model simulations (Lazhu et al., 2016; Ma et al., 2016;  
109 Li et al., 2017; Guo et al., 2019), owing to E neglect during the IC, the potential mechanisms of lake E  
110 and its different responses to climate change during the IC and IF remain unclear.

111 In this study, based on six continuous years of direct measurements of lake E and energy exchange flux  
112 data obtained with the EC technique pertaining to QHL, the largest saline lake on the QTP, between 2014  
113 and 2019, we quantified the characteristics of energy interchange and E on diurnal, seasonal (IF, IC and  
114 cycle year: AN) and yearly time scales and identified the potential influencing factors of E during the IF  
115 and IC. In addition, combined with reanalysis climate datasets, a mass transfer model (MT model), and  
116 a model based on energy, temperature and WS (JH model) were calibrated and verified, with the optimal  
117 model chosen for the simulation of lake E and its response to climate change during the IF and IC from  
118 2003 to 2017. The results would highlight the importance and potential mechanisms of E during IC, and  
119 can be used as a reference to further improve hydrological models of alpine lakes.

## 120 **2. Materials and Methods**

### 121 **2.1. Site description and energy exchange flux and climate data**

122 QHL ( $36^{\circ}32' - 37^{\circ}15' N$ ,  $99^{\circ}36' - 100^{\circ}47' E$ , 3194 m a.s.l.), with an area of 4,432 km<sup>2</sup> and a catchment of  
123 29,661 km<sup>2</sup>, is the largest inland saline lake in China (Li et al., 2016). The average depth of the lake is  
124 26 m. The average salt content is 14.13 g L<sup>-1</sup>, and the pH ranges from 9.15 to 9.30. The hydrochemical  
125 type of the lake water is Na-SO<sub>4</sub>-Cl (Li et al., 2016). The mean annual  $T_a$ , precipitation, and E values  
126 between 1960 and 2015 were  $-0.1^{\circ}C$ , 355 mm and 925 mm, respectively (Li et al., 2016). The IC usually  
127 begins in late November, ends in mid-late March or even early April, and lasts more than 100 days.  
128 Under the effects of climate warming, QHL has experienced temperature increases, area expansion, and  
129 IC shortening.

130 The instruments to measure the energy exchange flux and micrometeorological parameters were installed



---

131 at the China Torpedo Qinghai Lake test base (36°35'27.65" N, 100°30'06" E, 3198 m a.s.l.) located in  
132 the southeastern QHL approximately 737 m from the nearest shore (Li et al., 2016) (Fig. 1). The water  
133 depth underneath this platform is 18 m. The torpedo test tower has a height of 10 m above the water  
134 surface. The EC system was installed on a steel pillar mounted on the northwestern side of the top of the  
135 torpedo test tower with a total height of 17.3 m above the lake water surface (Li et al., 2016). A three–  
136 dimensional sonic anemometer (model CSAT3, Campbell Scientific Inc., Logan, UT, USA) was used to  
137 directly measure horizontal and vertical wind velocity components ( $u$ ,  $v$ , and  $w$ ) and virtual temperature.  
138 An open–path infrared gas analyzer (model EC150, Campbell Scientific Inc.) was applied to measure  
139 fluctuations in water vapor and carbon dioxide concentrations. Fluxes of sensible heat ( $H$ ) and latent heat  
140 ( $LE$ ) were calculated from the 10–Hz time series at 30–min intervals and recorded by a data logger  
141 (CR3000, Campbell Scientific Inc.). The observation instruments were powered by solar energy.

142 A suite of auxiliary micrometeorology was also measured as 30–min averages of 1–s readings on the  
143 eastern side of the top of the torpedo test tower, 3 m away from the EC instruments. The net radiation  
144 ( $R_n$ ) was calculated from the incoming shortwave, reflected shortwave, and incoming and outgoing  
145 longwave radiation, which were measured by a net radiometer (CNR4, Kipp & Zonen B.V., Delft,  
146 Netherlands) at 10 m above the lake surface (Fig. 1). The  $T_a$ , relative humidity (RH) and air pressure  
147 ( $P_{res}$ ) were measured at a height of 12.5 m above the water surface. A wind sentry unit (model 05103,  
148 RM Young, Inc. Traverse City, MI, USA) was employed to measure the WS and wind direction (WD).  
149 The  $T_s$  was measured with an infrared thermometer (model SI–111, Campbell Scientific Inc.)  
150 approximately 10 m above the water surface, and the water temperature ( $T_l$ ) was measured with a  
151 temperature probe (109 L, Campbell Scientific Inc.) at depths of 0.2, 0.5, 1.0, 2.0 and 3.0 m. precipitation  
152 was measured with an automated tipping–bucket rain gauge (model TE525, Campbell Scientific Inc.)  
153 and precipitation gauge (model T–200B, Campbell Scientific Inc.). The observation system began  
154 operation on May 11, 2013. In this study, we unified all observational data at 30–min intervals and  
155 analyzed the data from January 1, 2014 to December 31, 2019.

## 156 2.2. Reanalysis climate datasets

157 The reanalysis climate datasets used to drive the lake E models were acquired from the interim reanalysis  
158 dataset v5 (ERA5) produced by the European Centre for Medium–Range Weather Forecasts



159 (<https://cds.climate.copernicus.eu/cdsapp#!/search?type=dataset>) and the China Regional High-  
160 Temporal-Resolution Surface Meteorological Elements-Driven Dataset (CMFD)  
161 (<http://data.tpdc.ac.cn/en/>). Gridded hourly ERA5 skin temperature and daily WS, daily CMFD Ta, Pres,  
162 RH, and downward shortwave radiation (Rs) at a spatial resolution of 0.1° from 2001 to 2018 were  
163 analyzed in this study. The daily skin temperature was generated by averaging the hourly temperature  
164 over 24 h per day and was adopted as the lake surface temperature. We extracted climate data pertaining  
165 to QHL via a grid mask with a spatial resolution of 0.1° and averaged the data in all pixels. Considering  
166 the advantages of long time spans and high resolution, the ERA5 and CMFD datasets developed based  
167 on land station data have been recognized as the best currently available reanalysis products and have  
168 been widely applied in land-surface and hydrological modelling studies in China (Lazhu et al., 2016; Ma  
169 et al., 2016; Tian et al., 2021; Xiao and Cui, 2021). To reduce the uncertainty caused by the input data,  
170 the daily lake surface temperature from EAR5, Ta and Rs from CMFD for QHL were adjusted with fitting  
171 equations of the observed daily Ts ( $R^2 = 0.92$ ,  $P < 0.01$ ), Ta ( $R^2 = 0.90$ ,  $P < 0.01$ ) and Rs ( $R^2 = 0.73$ ,  $P <$   
172  $0.01$ ) from 2014 to 2018 (Fig. S1), and the equations were shown as below:

$$173 \quad T_a^{ad} = 1.01 \times T_a^{CMFD} + 0.71 \quad (1)$$

$$174 \quad T_s^{ad} = 0.71 \times T_s^{ERA5} + 3.30 \quad (2)$$

$$175 \quad R_s^{ad} = 0.86 \times R_s^{CMFD} + 34.63 \quad (3)$$

176 where  $T_a^{ad}$ ,  $T_s^{ad}$  and  $R_s^{ad}$  are Ta, Ts and Rs, respectively, after adjustment.

### 177 2.3. Lake ice coverage dataset and ice phenology

178 The daily lake ice coverage of QHL from 2002 to 2018 was extracted from a lake ice coverage dataset  
179 of 308 lakes (with an area greater than 3 km<sup>2</sup>) on the QTP retrieved from the National Tibetan Plateau  
180 Data Center (<http://data.tpdc.ac.cn/en/>). The dataset with a time span from 2002 to 2018 was generated  
181 from the Moderate Resolution Imaging Spectroradiometer (MODIS) normalized difference snow index  
182 (NDSI) product with the SNOWMAP algorithm, and the data under cloud cover conditions were  
183 redetermined based on the temporal and spatial continuity of lake surface conditions (Qiu et al., 2019).  
184 Based on the lake ice coverage, the IF was defined as an ice coverage lower than 10%, and the IC was  
185 defined as an ice coverage higher than 10% (Qiu et al., 2019). The IC was divided into three stages:



186 freeze (FZ: 10% < ice coverage < 90%), completely freeze (CF: ice coverage > 90%) and thaw (TW: 10%  
187 < ice coverage < 90%) (Qiu et al., 2019). We defined the cycle year (annual: AN) from the beginning of  
188 the IF to the end of the IC.

#### 189 **2.4 Data processing of the observed energy exchange flux and climate data**

190 The EC fluxes were processed and corrected based on the 10-Hz raw time series data in the data  
191 processing software EdiRe, including spike removal, lag correction of water to carbon dioxide relative  
192 to the vertical wind component, sonic virtual temperature correction, performance of planar fit coordinate  
193 rotation, density fluctuation correction (WPL correction) and frequency response correction (Li et al.,  
194 2016). Since the shortest distance between the Chinese torpedo Qinghai Lake test base and the  
195 southwestern lakeshore is only 737 m, there may be insufficient fetch for a turbulent flux under certain  
196 conditions. Therefore, footprint analysis was conducted to eliminate data influenced by the surrounding  
197 land. For further details on the process and results of the footprint analysis, see Li et al. (2016). In addition  
198 to these processing steps, quality control of the 30-min flux data was conducted using a five-step  
199 procedure: (i) data originating from periods of sensor malfunction were rejected (e.g., when there was a  
200 faulty diagnostic signal), (ii) data within 1 h before or after precipitation were rejected, (iii) incomplete  
201 30-min data were rejected when the missing data constituted more than 3% of the 30-min raw record,  
202 (iv) data were rejected at night when the friction velocity was below 0.1 m/s (Blanken et al., 1998) and  
203 (v) data with large footprints (>700 m) and a wind direction from 180° to 245° were eliminated.

204 To further control the quality of the energy exchange flux (sensible heat flux and latent heat flux: H and  
205 LE, respectively) and micrometeorological dataset (Rn, Ta, Ts, Tl, RH, WS, Pres, and albedo), data  
206 outside the mean  $\pm 3 \times$  standard deviation were removed for each variable. Then, gap-filling methods  
207 entailing a look-up table and mean diurnal variation (Falge et al., 2001) were adopted to fill gaps in the  
208 flux measurement data. The look-up table method was applied when the meteorological dataset was  
209 available synchronously. Otherwise, the mean diurnal variation method was adopted. The heat storage  
210 change ( $G$ ,  $W/m^2$ ) was estimated as a residual of the energy balance:

$$211 \quad G = R_n - LE - H \quad (4)$$

212 where  $R_n$  is the net radiation ( $W/m^2$ ),  $H$  is the sensible heat flux ( $W/m^2$ ) and  $LE$  is the latent heat flux  
213 ( $W/m^2$ ). Lake E was calculated as



---

$$214 \quad E = \lambda \times LE \quad (5)$$

215 where  $\lambda$  is the latent heat of vaporization (MJ/kg), taken as 2.45 MJ/kg in this paper (Allen et al.,  
216 1998).

### 217 2.5. Models for daily lake evaporation simulation

218 To evaluate the interannual variation in QHL E from 2003 to 2017, we validated three models during the  
219 AN, IF, and IC periods. The three models were as follows:

220 1) Mass–transfer model (MT model) (Harbeck et al., 1958)

$$221 \quad E_{MT} = N \times F(WS) \times \Delta e \quad (6)$$

$$222 \quad F(WS) = a1 \times WS + a2 \quad (7)$$

$$223 \quad \Delta e = \alpha \times e_s - e_a \quad (8)$$

$$224 \quad e_s = 6.105 \times \exp\left(\frac{17.27 \times T_s}{T_s + 237.7}\right) \quad (9)$$

$$225 \quad e_a = 6.105 \times \exp\left(\frac{17.27 \times T_a}{T_a + 237.7}\right) \quad (10)$$

226 where  $E_{MT}$  is the E rate (mm/day);  $N$  is the mass–transfer coefficient;  $WS$  is the wind speed (m/s);  $\Delta e$   
227 is the vapor pressure difference and  $\alpha$  is the water activity coefficient for saline lakes, which represents  
228 the ratio between the vapor pressure above saline water and that above freshwater at the same temperature,  
229 and an  $\alpha$  value of 0.97 was suggested for QHL, as measured with a portable water activity meter  
230 (AwTester, China). Moreover,  $e_s$  and  $e_a$  are the saturated vapor pressure at the lake surface  
231 temperature ( $T_s$ ) and air temperature ( $T_a$ ), respectively. This model inherently accounts for the water  
232 salinity through  $\Delta e$  and requires calibration of coefficients  $N$ ,  $a1$  and  $a2$ , which were taken as 1.86, 0.01,  
233 and 0.13, respectively, during the AN; 0.18, 0.40, and 0.26, respectively, during the IF; and 0.97, 0.09,  
234 and 0.38, respectively, during the IC in this paper.

235 2) Atmospheric dynamics model (AD model) (Hamdani et al., 2018)

$$236 \quad E_{AD} = \frac{0.622 \times C_e}{\rho_w \times P} \times \rho_a \times WS \times 3.6 \times 10^6 \times \Delta e \quad (11)$$



---

$$237 \quad \rho_a = 1.293 \times \left( \frac{273.15}{273.15 + T_a} \right) \times \frac{Pres}{101.325} \quad (12)$$

238 where  $\rho_w$  and  $\rho_a$  denote the water and air densities ( $\text{kg/m}^3$ ), respectively, and  $\rho_w$  is approximately  
239  $1.011 \times 10^3$  for QHL. Moreover,  $Pres$  is the air pressure (mbar), and  $Ce$  is a transport coefficient  
240 obtained via calibration to address missing friction velocity values in the reanalysis climate datasets,  
241 which was taken as  $3.20 \times 10^{-3}$ ,  $3.00 \times 10^{-3}$  and  $6.60 \times 10^{-3}$  during the AN, IF and IC, respectively, in  
242 this paper.

243 3) Statistical model based on solar radiation (the Jensen–Haise method: JH model) (Wang et al., 2019a)

$$244 \quad E_{JH} = JH1 \times (JH2 \times (T_a - T_s) + JH3) \times (Rs) \times (WS) \quad (13)$$

245 where  $Rs$  is the incoming solar shortwave radiation ( $\text{W/m}^2$ );  $JH1$ ,  $JH2$  and  $JH3$  must be calibrated and  
246 were taken as  $6.80 \times 10^{-3}$ ,  $-0.01$  and  $0.38$ , respectively, during the AN;  $0.03$ ,  $-3.80 \times 10^{-3}$  and  $0.08$ ,  
247 respectively, during the IF; and  $6.90 \times 10^{-3}$ ,  $0.02$  and  $0.49$ , respectively, during the IC in this paper.

248 The three models were selected, firstly as they are typical representatives in considering mass transfer,  
249 aerodynamics, energy transfer, respectively; secondly because their demand parameters are easy to  
250 acquire, which are adaptive to be promoted; and third as they have been proved to be efficient in saline  
251 lakes (Hamdani et al., 2018). These models were first calibrated and validated based on daily  $E$   
252 observations from 2014 to 2019 during the different periods of the AN, IF and IC. The root–mean–square  
253 error (RMSE) and goodness of fit ( $R^2$ ) were used to evaluate the effectiveness of the models. A model  
254 with high  $R^2$  and low RMSE values was selected for lake E simulation during the AN, IF and IC periods.

## 255 2.6. Statistical analysis

256 Summer and autumn were taken as June to August and September to November, respectively. During  
257 data analysis, we first divided the 30–min observed energy exchange flux and climate data from 2014 to  
258 2019 by the AN, IF, and IC based on the calculated ice phenology. Hence, we obtained datasets of five  
259 cycle years from the IF in 2014 to the IC in 2018 (Fig. S2). Second, we calculated the multiday average  
260 30–min observed energy exchange flux during the IF and IC in each year to evaluate the basic statistical  
261 characteristics of the diurnal  $E$  and exchange flux. The daily energy exchange flux and climate data were  
262 then calculated by averaging the 30–min data for each day, and one–way ANOVA was performed to



263 compare the difference in E and G between the IF and IC in each year from 2014 to 2018. Third, to  
264 explore the key factor controlling lake E, partial least squares regression and random forest methods were  
265 used to calculate the sensitivity coefficient (standing for the regression coefficient of each variable, which  
266 means the amount of change in E caused by the variation of per unit in the variable) and importance of  
267  $R_n$ , WS,  $\Delta e$ , Pres, albedo, WD,  $T_a - T_s$ , TI, and ICR to E during the daytime and nighttime IF and IC,  
268 respectively. Finally, three models were validated and two models were selected to severally calculate  
269 the interannual E during the IF and IC from 2003 to 2017 (the available ice phenology exhibits a limited  
270 cycle year from 2003 to 2017). Four controlled tests were then conducted to quantify the contribution of  
271 the variation in  $T_a$ ,  $T_s$ , WS, and  $R_s$  to lake E from 2003 to 2017. The partial least squares and random  
272 forest analyses were conducted in R and the other analyses were conducted in MATLAB.

### 273 3. Results

#### 274 3.1. Diurnal and seasonal characteristics of evaporation and the energy budget during the different 275 freeze–thaw periods

276 The average E, LE, G, H, and  $R_n$  values (average from 2014 to 2018) were  $1.20 \pm 0.09$  mm/d,  $68.01 \pm$   
277  $4.93$  W/m<sup>2</sup>,  $192.18 \pm 7.00$  W/m<sup>2</sup>,  $16.25 \pm 1.21$  W/m<sup>2</sup> and  $276.45 \pm 3.32$  W/m<sup>2</sup>, respectively, during the  
278 IF; and  $1.11 \pm 0.20$  mm/d,  $63.15 \pm 11.31$  W/m<sup>2</sup>,  $79.23 \pm 18.12$  W/m<sup>2</sup>,  $4.68 \pm 0.37$  W/m<sup>2</sup> and  $147.06 \pm$   
279  $14.23$  W/m<sup>2</sup>, respectively, during the IC. The daytime E, LE, G, H and  $R_n$  values were notably lower  
280 during the IC than those during the IF, except E and LE in 2014 (Figs. 2 and 3; Table S1). In addition,  
281 the daily peak LE and E values typically occurred at approximately 12 pm during the IF and  
282 approximately 2 pm during the IC, and exhibited an approximately two–hour lag during the IF and a  
283 four–hour lag during the IC over G and  $R_n$  (Fig. 2). At night, although lower E (at an average rate of  $0.81$   
284  $\pm 0.17$  mm/d) and LE ( $46.02 \pm 9.71$  W/m<sup>2</sup>) levels occurred during the IC than during the IF (at average  
285 rates of  $0.94 \pm 0.05$  mm/d and  $53.09 \pm 2.94$  W/m<sup>2</sup>, respectively), E (LE) accounted for 42%–45% and  
286 41%–45% of the total daily E during the IF and IC, respectively (Figs. 2 and 3; Table S1). In regard to  
287 G, a similar release rate was found during the IF and IC, but the heat release time was longer during the  
288 IC than that during the IF (Fig. 2).

289 The daily E ranged from 1.96 to 2.34 mm/d during the IF and from 1.57 to 2.71 mm/d during the IC, and



---

290 the average E sum reached  $593.37 \pm 44.87$  mm/yr during the IF and  $175.22 \pm 45.98$  mm/yr during the IC  
291 from 2014 to 2018 (Fig. 3; Fig. S2; Table S1). This suggests an average E sum of 77% during the IF and  
292 23% during the IC throughout the cycle year from 2014 to 2018 (with a lake E sum ranging from 719.45  
293 to 798.55 mm/yr and an average value of  $768.58 \pm 28.73$  mm/yr) (Fig. 3). In terms of G, QHL initially  
294 released heat in autumn, which lasted until the lake was completely frozen, after which heat was absorbed  
295 from the lake thawing period throughout the summer (Fig. S2; Fig. S3).

### 296 3.2. Response of evaporation to climatic factors during the different freeze–thaw periods

297 The key controlling factor of lake E was explored based on the daily observed energy exchange flux and  
298 climate data (E, Rn, WS,  $\Delta e$ , Pres, albedo, WD,  $T_a - T_s$ , and Tl) and ICR during the IF and IC from 2014  
299 to 2018. The  $\Delta e$  (with a sensitivity coefficient of 0.28 in the daytime and 0.22 in the nighttime,  $P < 0.05$ ),  
300 WS (with a sensitivity coefficient of 0.54 in the daytime and 0.43 in the nighttime,  $P < 0.05$ ) and Pres  
301 (with a sensitivity coefficient of 0.26 in the daytime and 0.14 in the nighttime,  $P < 0.05$ ) notably increased  
302 E (Fig. 4), and the effect was greater in the daytime than that in the nighttime during the IF (Fig. 4). The  
303 Rn (with a sensitivity coefficient 0.25 in the nighttime,  $P < 0.05$ ), WS (with a sensitivity coefficient of  
304 0.30 in the daytime and 0.22 in the nighttime,  $P < 0.05$ ),  $T_a - T_s$  (with a sensitivity coefficient of 0.59 in  
305 the daytime and 0.39 in the nighttime,  $P < 0.05$ ) and ICR (with a sensitivity coefficient of 0.20 in the  
306 daytime and 0.17 in the nighttime,  $P < 0.05$ ) imposed a significant positive effect on E during the IC (Fig.  
307 4). Similarly, the top five important factors calculated with the random forest method were WS,  $\Delta e$ , Pres,  
308 WD, and  $T_s$  during the IF and  $T_a - T_s$ ,  $T_a$ , WS, Rn, and ICR during the IC (Fig. S4). This indicates that E  
309 of QHL is mainly controlled by WS,  $\Delta e$ , and Pres during the IF but is driven by Rn,  $T_a - T_s$ , WS, and ICR  
310 during the IC.

### 311 3.3. Evaporation simulation and interannual variation

312 Three models (MT, AD, and JH) were calibrated and validated to evaluate the interannual variation in  
313 QHLE from 2003 to 2017. In the case of model performance, the MT model based on molecular diffusion  
314 performed the best in terms of E simulation during the IF (with the largest  $R^2$  and smallest RMSE values  
315 of 0.77 and 0.88, respectively), while the JH model based on energy exchange performed the best during  
316 the IC (with the largest  $R^2$  and smallest RMSE values of 0.68 and 1.07, respectively) (Figs. S5 and S6).  
317 Thus, the interannual variation in QHL E from 2003 to 2017 was calculated with the MT model during



---

318 the IF and with the JH model during the IC (Fig. 5). From 2003 to 2017, although  $T_a$  (at a rate of  
319  $-0.01^\circ\text{C}/\text{yr}$ ),  $P_{\text{res}}$  (at a rate of  $-0.01 \text{ hPa}/\text{yr}$ ) and  $WS$  (at a rate of  $-0.006 \text{ m}/(\text{s}\cdot\text{yr})$ ) decreased, increases  
320 in  $\Delta e$  (at a rate of  $0.01 \text{ hPa}/\text{yr}$ ) and  $T_s$  (at a rate of  $0.001^\circ\text{C}/\text{yr}$ ) resulted in an increase in  $E$  (at a rate of  
321  $1.49 \text{ mm}/\text{yr}$  for the  $E$  sum) during the IF (Figs. 5 and S7). Conversely, ignoring the increases in  $T_a$  (at a  
322 rate of  $0.04^\circ\text{C}/\text{yr}$ ) and  $T_a - T_s$  (at a rate of  $0.04^\circ\text{C}/\text{yr}$ ), with decreasing  $WS$  (at a rate of  $-0.008 \text{ m}/(\text{s}\cdot\text{yr})$ ),  
323  $E$  (at a rate of  $-1.96 \text{ mm}/\text{yr}$  for the  $E$  sum) decreased during the IC, which resulted in an inapparent  
324 decrease in  $E$  (at a rate of  $-0.46 \text{ mm}/\text{yr}$  for the  $E$  sum) during the AN (Figs. 5 and S7).

## 325 4. Discussion

### 326 4.1. Lake evaporation during the ice-covered period

327 The results of this study highlight the important contribution of lake ice sublimation to the total amount  
328 of lake  $E$ . Due to the low snow coverage of Qinghai Lake in winter (with a maximal snow coverage less  
329 than 16% of the area of Qinghai Lake), evaporation and sublimation of lake ice and water are the main  
330 sources of  $E$  during the IC of 2013–2018 (Fig S8). In liquid drops,  $E$  can be explained based on the  
331 coffee-stain effect in which the local diffusion-limited  $E$  rate diverges at the contact line (the border of  
332 the liquid drops) and outward flow from a given droplet replenishes the corner region if the droplet  
333 contact line remains fixed (Deegan et al., 1997 and 2000). Similarly, ice crystal  $E$  also starts at the contact  
334 line first and quickly recedes along sharp crystal edges (Nelson, 1998; Jambon-Puillet et al., 2018). Since  
335 the mass loss caused by  $E$  cannot be replaced, the occurrence of  $E$  at sharp points causes these points to  
336 successively retreat, resulting in self-similar smoothness (Jambon-Puillet et al., 2018). The experimental  
337 and simulation results of Jambon-Puillet et al. (2018) verified that the  $E$  rates of liquid droplets and ice  
338 crystals remain the same under unchanged environmental conditions. In this study, the  $E$  rate of QHL  
339 during the IC ranged from 1.57 to 2.71 mm/d, approximately 0.73–1.38 times that of liquid water during  
340 the IF (Table S1), with similar results to those findings of liquid droplets and ice crystals.

341 In practice, lake  $E$  varies diurnally, seasonally, and interannually with climatic and environmental  
342 changes, and the  $E$  rate varies considerably among lakes in different regions. Few studies have examined  
343 lake ice  $E$  during the IC, and most studies have focused on polar sea ice and alpine snow packs (Froyland  
344 et al., 2010; Froyland, 2013; Herrero et al., 2016; Christner et al., 2017; Lin et al., 2020). Observational



345 and modelling studies of Antarctic ice sheets or lakes have found that the monthly E rate of ice ranged  
346 from  $-4.6$  to  $13$  mm/month from June to September (Antarctic) (Froyland et al., 2010). In this study, we  
347 found that E sum ranges from  $130.59$  to  $262.45$  mm during the IC from 2014 to 2018, which is higher  
348 than the previous observations from Antarctic ice sheets or lakes. This may be because Antarctic ice  
349 sheets or lakes are located at high latitudes with low solar radiation and are therefore cooler from the  
350 surface to greater depths with energy-limiting conditions for E (Persson et al., 2002). However, the lakes  
351 on the QTP freeze seasonally, so most of these lakes can store a large amount of heat because of the high  
352 solar radiation during the IF (Fig. 6), which could lead to the observed E during the IC (Huang et al.,  
353 2011 and 2016). Studies on surface E of a shallow thermokarst lake in the central QTP region have found  
354 that E reaches up to  $250$  mm/yr during the IC (Huang et al., 2016), which is close to our observed E  
355 levels ( $130.59$ – $262.45$  mm/yr). Our results further showed that E of QHL accounted for 23% of the  
356 annual E during the IC. Wang et al. (2020) evaluated 75 large lakes on the QTP and demonstrated that E  
357 of these lakes in winter accounted for 12.3%–23.5% of the annual E, which suggests that E of these lakes  
358 during the IC was the same as that during the other seasons. Furthermore, considering that the area of  
359 QHL is  $4,432$  km<sup>2</sup> (Li et al., 2016), the QHL releases  $3.39 \pm 0.13$  km<sup>3</sup> of water into the air every year,  
360 which corresponds to the sum of the water for animal husbandry, industrial and domestic uses in Qinghai  
361 province (an average of 2014 to 2017) (Dong et al., 2021).

#### 362 **4.2. Responses of lake evaporation to salinity and climate change**

363 The salinity has a powerful influence on E of saline lakes by changing both water density and thermal  
364 property, dissolved salt ions can reduce the free energy of water molecules, and result in a higher boiling  
365 point and reduced saturated vapor pressure above saline lakes at a given water temperature (Salhotra et  
366 al., 1987; Abdelrady, 2013; Mor et al., 2018). Therefore, increase in salinity of lake would decrease its E  
367 rate. For example, Lee (1927) compared the E of pure water with that of saline lakes of different densities  
368 (salinity) in Nevada, USA, and found that when the densities (salinity) of water increased by 1%, the E  
369 of saline lake decreased by 0.01% compared with pure water. Similarly, Mor et al. (2018) found that E  
370 rate of diluted plume is nearly three times larger than that in open lake in Dead Sea. Thus, the  
371 thermodynamic concept of water activity (the water activity of freshwater is 1, while in saline water is  
372 lower than 1, and the higher the salinity, the lower of water active in lakes.) has been widely used in E



373 simulations of saline lakes, which is defined as the ratio of water vapor pressure on the surface of saline  
374 and fresh water at a given temperature (Salhotra et al., 1987; Abdelrady, 2013; Mor et al., 2018). In our  
375 study, we measured the water activity of QHL was 0.97 by a salinity of  $14.13 \text{ g L}^{-1}$ , and applied it to the  
376 models, which make it more theoretical to explain E process of saline lakes and reduced the uncertainty  
377 of estimation in saline lake E. For example, with the salinity of  $133 \text{ g L}^{-1}$  of surface water, water activity  
378 was measured to be 0.65, and has been widely used in its E simulation of Dead sea (Metzger et al., 2018;  
379 Mor et al., 2018; Lensky et al., 2018); and Abdelrady (2013) improved the surface energy balance system  
380 (SEBS) of E in saline lakes by constructing an exponential function between lake salinity and water  
381 activity, which reduced the simulated E by 27% and RMSE from  $0.62$  to  $0.24 \text{ mm 3h}^{-1}$  in the Great Salt  
382 Lake. Therefore, considering salinity is very important to improve the accuracy of E simulation in saline  
383 lakes. Certainly, lake salinity changes dynamically at diurnal, seasonal and interannual scales, but since  
384 the difficult of continuously observation of lake salinity, a fixed water activity in our study may cause  
385 the underestimate in E of QHL, due to the decrease of salinity by the expansion of QHL.

386 Furthermore, climate and environment are also important factors affecting lake E, and varied  
387 significantly among the different seasons. Previous studies have shown that lake E is mainly affected by  
388 WS and  $\Delta e$  in summer and WS,  $\Delta e$ ,  $T_a - T_s$ , and G in winter (Zhang and Liu, 2014; Hamdani, et al., 2018).  
389 This suggests that energy exchange between lakes and air may be one of the main drivers of E during the  
390 IC under the same atmospheric boundary conditions (Fig. 6). Since most lakes store heat in summer, they  
391 release heat and sufficiently produce E in winter (Blanken et al., 2011; Hamdani, et al., 2018). In this  
392 study, we also found that QHL began to store heat in the lake thawing period and released heat in autumn  
393 or when the lake began to freeze (Figs. 6 and S3). Therefore, E of QHL was mainly controlled by WS,  
394  $\Delta e$ , and Pres during the IF, whereas it was mainly affected by  $R_n$ ,  $T_a - T_s$  and WS during the IC (Fig. 6).

395 Considering the overall surface air warming and moistening, solar dimming, and wind stilling since the  
396 beginning of the 1980s across the QTP (Yang et al., 2014), we further explored the contribution of  $T_a$ ,  
397  $T_s$ , WS and  $R_s$  to E during the IF and IC from 2001 to 2017 by simulation tests. Compared with 2001, E  
398 during the IC increased at an average rate (2003–2017) of  $4.90 \pm 6.14 \text{ mm/yr}$  (3.52%) due to an increase  
399 in  $T_a$  and decreased at an average rate (2003–2017) of  $-5.84 \pm 3.54 \text{ mm/yr}$  (3.37%),  $-6.17 \pm 4.77 \text{ mm/yr}$   
400 (3.19%), and  $-18.92 \pm 27.55 \text{ mm/yr}$  (11.14%) due to an increase in  $T_s$  and decrease in  $R_s$  and WS,



---

401 respectively (Fig. 7; Table S2). Moreover, the increase in  $T_s$  increased  $E$  at an average rate (2003–2017)  
402 of  $10.19 \pm 19.00$  mm/yr (3.37%) during the IF (Fig. 7; Table S2). In addition, changes in lake ice  
403 phenology significantly affected lake  $E$  during the IF and IC. Compared with 2003 to 2007 ( $101.40 \pm$   
404  $7.00$  d), the average IC decreased by 10.8 d from 2013 to 2017 ( $90.60 \pm 6.08$  d) (Table S3). A shortened  
405 IC suggests a much lower albedo in the cycle year and could result in higher  $R_s$  absorption and a shorter  
406 period for heat-induced recession, which could increase lake  $E$  (Wang et al., 2018). Of course, lake  $E$  is  
407 also affected by the lake area, water level, and physical and chemical properties (Woolway et al., 2020),  
408 especially for saline lakes (Salhotra et al., 1987; Mohammed and Tarboton, 2012; Mor et al., 2018).  
409 Increasing the water salinity could reduce  $E$  (Salhotra et al., 1987; Mor et al., 2018) because the dissolved  
410 salt ions could reduce the free energy of water molecules (i.e., reduced water activity) and result in a  
411 lower saturated vapor pressure above saline lakes at a given water temperature (Salhotra et al., 1987;  
412 Mor et al., 2018). However, the changes in lake physical and chemical properties attributed to lake  
413 freezing increase the complexity of the underlying mechanism, simulation of ice  $E$  and its response to  
414 climate change, and more studies are needed to further explore interactions between the different factors.

#### 415 4.3. Uncertainty

416 Based on six continuous year-round direct measurements of lake  $E$  and energy exchange flux, we  
417 determined the  $E$  loss during the IC and calibrated and verified different models for  $E$  simulation during  
418 the IF and IC. Due to the lack of accurate measurements of deep lake temperature, energy budget closure  
419 ratios of EC observations in QHL are not given in this study. EC measurements have been widely used  
420 to quantify the  $E$  of several global lakes, including Lake Superior in America, Great Slave lake in Canada,  
421 Lake Geneva in Switzerland, Lake Valkea–Kotinen in Finland, and Taihu Lake, Erhai Lake, Poyang Lake,  
422 Nam Co, Selin Co and Ngoring Lake in China (Blanken et al., 2000; Vercauteren et al., 2009; Blanken  
423 et al., 2011; Nordbo et al., 2011; Wang et al., 2014; Li et al., 2015; Liu et al., 2015; Guo et al., 2016; Li  
424 et al., 2016; Ma et al., 2016; Lensky et al., 2018). With the most of the known energy budget closure  
425 ratios is over 0.7, EC observation of lakes is regarded as an accurate and reliable direct measurement  
426 method of  $E$ , even in lakes over QTP (Wang et al., 2020). Certainly, compared with land stations, the  
427 energy budget closure ratios over lake surfaces can be significantly influenced by the large amount of  
428 heat storage (release) during different seasons (Wang et al., 2020), which would increase the uncertainty



---

429 about the quantification of E. Besides, quantification of E during the IC depends on accurate ice  
430 phenology identification, and a longer IC suggests more E. Therefore, the different data sources and  
431 phenological classification methods of ice phenology comprise one source of uncertainty. In addition,  
432 we examined the sensitivity of the input variables (Ta, Ts, Rs and WS) of the chosen model. Increases in  
433 Ta, Ts, Rs, and WS of 10% could result in changes of -2.25%, 1.78%, 10.00% and 10.00% in the  
434 simulated E during the IC, respectively, indicating that E is more sensitive to Rs and WS than Ta and Ts  
435 in the JH model during the IC (Fig. S9). Moreover, the simulated E is minimally sensitive to Ta, and a  
436 10% increase in WS could result in a change of 8.54% in the simulated E during the IF, while a change  
437 in Ts could lead to an exponential change in the simulated E (Fig. S9).

## 438 **5. Conclusions**

439 In summary, based on six continuous year-round 30-min direct flux measurements throughout the cycle  
440 year from 2014 to 2018, the night E of QHL occupied over 40% during both the IF and IC. With a  
441 multiyear average of  $175.22 \pm 45.98$  mm/yr, E during the IC accounted for 23% of the total cycle year E  
442 sum, which is an important component in calculating E of saline lakes. A difference-based control factor  
443 of E was also found during the IF and IC. E of QHL was mainly controlled by atmospheric dynamic  
444 factors (WS,  $\Delta e$ , and P) during the IF, whereas it was driven by both energy exchange and atmospheric  
445 boundary conditions ( $R_n$ ,  $T_a - T_s$  and WS) during the IC. Thus, the MT model based on molecular  
446 diffusion performed best in lake E simulation during the IF, while the JH model based on energy exchange  
447 performed best during the IC. Furthermore, simulation of the E of QHL showed a slight decrease from  
448 2003 to 2017, caused by a decrease in E during the IC, and WS weakening may have resulted in an  
449 average reduction of 11.1% in lake E during the IC from 2003 to 2017. Our results suggest that E during  
450 the IC is non-negligible for saline lake E, and E simulation should be further improved in future model  
451 simulation studies, considering the difference in its potential mechanisms during the IC.

## 452 **Author Contributions**

453 XY Li conceived the idea, FZ Shi performed the analyses. XY Li, FZ Shi, DL Chen and YJ Ma led the  
454 manuscript writing. SJ Zhao, YJ Ma, JQ Wei and QW Liao provided analysis of datasets. All contributed  
455 to review and revise the manuscript.



---

456 **Acknowledgements**

457 The study was financially supported by the National Natural Science Foundation of China  
458 (NSFC: 41971029), the Second Tibetan Plateau Scientific Expedition and Research Program  
459 (STEP, grant no. 2019QZKK0306), the State Key Laboratory of Earth Surface Processes and  
460 Resource Ecology (2021–ZD–03) and Ten Thousand Talent Program for leading young  
461 scientists and the China Scholarship Council. The gridded climate datasets from the interim  
462 reanalysis dataset v5 (ERA5) produced by the European Centre for Medium–Range Weather  
463 Forecasts (<https://cds.climate.copernicus.eu/cdsapp#!/search?type=dataset>) and the China  
464 Regional High–Temporal–Resolution Surface Meteorological Elements–Driven Dataset  
465 (CMFD) (<http://data.tpdc.ac.cn/en/>) can be freely accessed. The daily lake ice coverage data  
466 were retrieved from the National Tibetan Plateau Data Center (<http://data.tpdc.ac.cn/en/>).

467 **Competing interests**

468 The contact author has declared that none of the authors has any competing interests.



469

470 **References**

- 471 Abdelrady, A. R. Evaporation over fresh and saline water using SEBS. 2013. Master's Thesis. University  
472 of Twente.
- 473 Allen, R. G., Pereira, L. S., Raes, D., & Smith, M. (1998). Crop evapotranspiration—Guidelines for  
474 computing crop water requirements—FAO Irrigation and drainage paper 56. Fao, Rome, 300(9), D05109.
- 475 Blanken, P. D., Black, T. A., Neumann, H. H., Den Hartog, G., Yang, P. C., Nesic, Z., ... & Novak, M. D.  
476 (1998). Turbulent flux measurements above and below the overstory of a boreal aspen forest. *Boundary–*  
477 *Layer Meteorology*, 89(1), 109–140.
- 478 Blanken, P. D., Rouse, W. R., Culf, A. D., Spence, C., Boudreau, L. D., Jasper, J. N., ... & Verseghy, D.  
479 2000. Eddy covariance measurements of evaporation from Great Slave lake, Northwest Territories,  
480 Canada. *Water Resources Research*, 36(4): 1069–1077.
- 481 Blanken, P. D., Spence, C., Hedstrom, N., & Lenters, J. D. (2011). Evaporation from Lake Superior: 1.  
482 Physical controls and processes. *Journal of Great Lakes Research*, 37(4), 707–716.
- 483 Bowen, I. S. (1926). The ratio of heat losses by conduction and by evaporation from any water surface.  
484 *Physical Review*, 27(6), 779.
- 485 Cai, Y., Ke, C. Q., Li, X., Zhang, G., Duan, Z., & Lee, H. (2019). Variations of lake ice phenology on the  
486 Tibetan Plateau from 2001 to 2017 based on MODIS data. *Journal of Geophysical Research:*  
487 *Atmospheres*, 124(2), 825–843.
- 488 Christner, E., Kohler, M., & Schneider, M. (2017). The influence of snow sublimation and meltwater  
489 evaporation on  $\delta D$  of water vapor in the atmospheric boundary layer of central Europe. *Atmospheric*  
490 *Chemistry and Physics*, 17(2), 1207–1225.
- 491 Dalton, J. (1802). Experimental essays on the constitution of mixed gases; on the force of stream or vapor  
492 from water and other liquids, both in a Torricellian vacuum and in air; on evaporation; and on the  
493 expansion of gases by heat. *Proceedings of Manchester Literary and Philosophical Society*, 5, 536–602.
- 494 Deegan, R. D., Bakajin, O., Dupont, T. F., Huber, G., Nagel, S. R., & Witten, T. A. (1997). Capillary flow  
495 as the cause of ring stains from dried liquid drops. *Nature*, 389(6653), 827–829.
- 496 Deegan, R. D., Bakajin, O., Dupont, T. F., Huber, G., Nagel, S. R., & Witten, T. A. (2000). Contact line  
497 deposits in an evaporating drop. *Physical review E*, 62(1), 756.
- 498 Dong, H., Feng, Z., Yang, Y., Li, P., & You, Z. (2021). Sustainability assessment of critical natural capital:  
499 a case study of water resources in Qinghai Province, China. *Journal of Cleaner Production*, 286, 125532.
- 500 Falge, E., Baldocchi, D., Olson, R., Anthoni, P., Aubinet, M., Bernhofer, C., ... & Wofsy, S. (2001). Gap  
501 filling strategies for defensible annual sums of net ecosystem exchange. *Agricultural and forest*  
502 *meteorology*, 107(1), 43–69.
- 503 Finch, J., & Calver, A. (2008). Methods for the quantification of evaporation from lakes. Prepared for



- 
- 504 the World Meteorological Organization's Commission for Hydrology, 1–41.
- 505 Froyland, H. K. (2013). Snow loss on the San Francisco peaks: Effects of an elevation gradient on evapo-  
506 sublimation (Doctoral dissertation, Northern Arizona University).
- 507 Froyland, H. K., Untersteiner, N., Town, M. S., & Warren, S. G. (2010). Evaporation from Arctic sea ice  
508 in summer during the International Geophysical Year, 1957–1958. *Journal of Geophysical Research:*  
509 *Atmospheres*, 115(D15).
- 510 Gross, M. 2017. The world's vanishing lakes. *Current Biology*, 27, 43–46. doi:  
511 10.1016/j.cub.2017.01.008.
- 512 Guo, Y., Zhang, Y., Ma, N., Song, H., & Gao, H. (2016). Quantifying surface energy fluxes and  
513 evaporation over a significant expanding endorheic lake in the central Tibetan Plateau. *Journal of the*  
514 *Meteorological Society of Japan*. Ser. II, 94, 453–465.
- 515 Guo, Y., Zhang, Y., Ma, N., Xu, J., & Zhang, T. (2019). Long-term changes in evaporation over Siling  
516 Co Lake on the Tibetan Plateau and its impact on recent rapid lake expansion. *Atmospheric research*, 216,  
517 141–150.
- 518 Hamdani, I., Assouline, S., Tanny, J., Lensky, I. M., Gertman, I., Mor, Z., & Lensky, N. G. (2018).  
519 Seasonal and diurnal evaporation from a deep hypersaline lake: The Dead Sea as a case study. *Journal of*  
520 *Hydrology*, 562, 155–167.
- 521 Harbeck, G. E. (1958). Water-loss investigations: Lake Mead studies (Vol. 298). US Government  
522 Printing Office.
- 523 Herrero, J., & Polo, M. J. (2016). Evapsublimation from the snow in the Mediterranean mountains of  
524 Sierra Nevada (Spain). *The Cryosphere*, 10(6), 2981–2998.
- 525 Huang, L., Liu, J., Shao, Q., & Liu, R. (2011). Changing inland lakes responding to climate warming in  
526 Northeastern Tibetan Plateau. *Climatic Change*, 109(3), 479–502.
- 527 Huang, W., Li, R., Han, H., Niu, F., Wu, Q., & Wang, W. (2016). Ice processes and surface ablation in a  
528 shallow thermokarst lake in the central Qinghai–Tibetan Plateau. *Annals of Glaciology*, 57(71), 20–28.
- 529 Jambon–Puillet, E., Shahidzadeh, N., & Bonn, D. (2018). Singular sublimation of ice and snow crystals.  
530 *Nature communications*, 9(1), 1–6.
- 531 Lazhu, Yang, K., Wang, J., Lei, Y., Chen, Y., Zhu, L., ... & Qin, J. (2016). Quantifying evaporation and  
532 its decadal change for Lake Nam Co, central Tibetan Plateau. *Journal of Geophysical Research:*  
533 *Atmospheres*, 121(13), 7578–7591.
- 534 Lee C.H. 1927. Discussion of “Evaporation on reclamation projects” by IE Houk. *Transactions of the*  
535 *American Society of Civil Engineers*, 90: 340–343.
- 536 Lensky, N. G., Lensky, I. M., Peretz, A., Gertman, I., Tanny, J., & Assouline, S. (2018). Diurnal Course  
537 of evaporation from the dead sea in summer: A distinct double peak induced by solar radiation and night  
538 sea breeze. *Water Resources Research*, 54(1), 150–160.
- 539 Li, B., Zhang, J., Yu, Z., Liang, Z., Chen, L., & Acharya, K. (2017). Climate change driven water budget



- 
- 540 dynamics of a Tibetan inland lake. *Global and Planetary Change*, 150, 70–80.
- 541 Li, X. Y., Ma, Y. J., Huang, Y. M., Hu, X., Wu, X. C., Wang, P., ... & Liu, L. (2016). Evaporation and  
542 surface energy budget over the largest high-altitude saline lake on the Qinghai-Tibet Plateau. *Journal of*  
543 *Geophysical Research: Atmospheres*, 121(18), 10–470.
- 544 Li, Z., Lyu, S., Ao, Y., Wen, L., Zhao, L., & Wang, S. 2015. Long-term energy flux and radiation balance  
545 observations over lake Ngoring, Tibetan Plateau. *Atmospheric Research*, 155: 13–25.
- 546 Lin, Y., Cai, T., & Ju, C. (2020). Snow evaporation characteristics related to melting period in a forested  
547 permafrost region. *Environmental Engineering & Management Journal (EEMJ)*, 19(3).
- 548 Liu, C., Zhu, L., Wang, J., Ju, J., Ma, Q., Qiao, B., ... & Kai, J. (2021). In-situ water quality investigation  
549 of the lakes on the Tibetan Plateau. *Science Bulletin*. 66(17): 1727–1730.  
550 <https://doi.org/10.1016/j.scib.2021.04.024>.
- 551 Liu, H., Feng, J., Sun, J., Wang, L., & Xu, A. (2015). Eddy covariance measurements of water vapor and  
552 CO<sub>2</sub> fluxes above the Erhai Lake. *Science China Earth Sciences*, 58(3), 317–328.
- 553 Ma, N., Szilagyi, J., Niu, G. Y., Zhang, Y., Zhang, T., Wang, B., & Wu, Y. (2016). Evaporation variability  
554 of Nam Co Lake in the Tibetan Plateau and its role in recent rapid lake expansion. *Journal of Hydrology*,  
555 537, 27–35.
- 556 Messager, M. L., Lehner, B., Grill, G., Nedeva, I., & Schmitt, O. (2016). Estimating the volume and age  
557 of water stored in global lakes using a geo-statistical approach. *Nature communications*, 7(1), 1–11.
- 558 Mohammed, I. N., & Tarboton, D. G. (2012). An examination of the sensitivity of the Great Salt Lake to  
559 changes in inputs. *Water Resources Research*, 48(11).
- 560 Mor, Z., Assouline, S., Tanny, J., Lensky, I. M., & Lensky, N. G. (2018). Effect of water surface salinity  
561 on evaporation: The case of a diluted buoyant plume over the Dead Sea. *Water Resources Research*, 54(3),  
562 1460–1475.
- 563 Nelson, J. (1998). Sublimation of ice crystals. *Journal of the atmospheric sciences*, 55(5), 910–919.
- 564 Nordbo, A., Launiainen, S., Mammarella, I., Leppäranta, M., Huotari, J., Ojala, A., & Vesala, T. 2011.  
565 Long-term energy flux measurements and energy balance over a small boreal lake using eddy covariance  
566 technique. *Journal of Geophysical Research: Atmospheres*, 116: D02119.
- 567 Persson, P. O. G., Fairall, C. W., Andreas, E. L., Guest, P. S., & Perovich, D. K. (2002). Measurements  
568 near the Atmospheric Surface Flux Group tower at SHEBA: Near-surface conditions and surface energy  
569 budget. *Journal of Geophysical Research: Oceans*, 107(C10), SHE–21.
- 570 Penman, H. L. (1948). Natural evaporation from open water, bare soil and grass. *Proceedings of the*  
571 *Royal Society of London. Series A. Mathematical and Physical Sciences*, 193(1032), 120–145.
- 572 Qiu, Y., Xie, P., Leppäranta, M., Wang, X., Lemmetyinen, J., Lin, H., & Shi, L. (2019). MODIS-based  
573 daily lake ice extent and coverage dataset for Tibetan Plateau. *Big Earth Data*, 3(2), 170–185.
- 574 Salhotra, A. M., Adams, E. E., & Harleman, D. R. (1987). The alpha, beta, gamma of evaporation from  
575 saline water bodies. *Water Resources Research*, 23(9), 1769–1774.



- 
- 576 Tian, W., Liu, X., Wang, K., Bai, P., & Liu, C. (2021). Estimation of reservoir evaporation losses for  
577 China. *Journal of Hydrology*, 596, 126142.
- 578 Vercauteren, N., Bou-Zeid, E., Huwald, H., Parlange, M. B., & Brutsaert, W. 2009. Estimation of wet  
579 surface evaporation from sensible heat flux measurements. *Water Resources Research*, 45(6): W06424.
- 580 Wan, W., Zhao, L., Xie, H., Liu, B., Li, H., Cui, Y., ... & Hong, Y. (2018). Lake surface water temperature  
581 change over the Tibetan plateau from 2001 to 2015: A sensitive indicator of the warming climate.  
582 *Geophysical Research Letters*, 45(20), 11–177.
- 583 Wang, B., Ma, Y., Chen, X., Ma, W., Su, Z., & Menenti, M. (2015). Observation and simulation of lake-  
584 air heat and water transfer processes in a high-altitude shallow lake on the Tibetan Plateau. *Journal of*  
585 *Geophysical Research: Atmospheres*, 120(24), 12327–12344.
- 586 Wang, B., Ma, Y., Wang, Y., Su, Z., & Ma, W. (2019a). Significant differences exist in lake-atmosphere  
587 interactions and the evaporation rates of high-elevation small and large lakes. *Journal of hydrology*, 573,  
588 220–234.
- 589 Wang, B., Ma, Y., Ma, W., Su, B., & Dong, X. (2019b). Evaluation of ten methods for estimating  
590 evaporation in a small high-elevation lake on the Tibetan Plateau. *Theoretical and applied climatology*,  
591 136(3), 1033–1045.
- 592 Wang, B., Ma, Y., Su, Z., Wang, Y., & Ma, W. (2020). Quantifying the evaporation amounts of 75 high-  
593 elevation large dimictic lakes on the Tibetan Plateau. *Science advances*, 6(26), eaay8558.
- 594 Wang, W., Lee, X., Xiao, W., Liu, S., Schultz, N., Wang, Y., ... & Zhao, L. (2018). Global lake evaporation  
595 accelerated by changes in surface energy allocation in a warmer climate. *Nature Geoscience*, 11(6), 410–  
596 414.
- 597 Wang, W., Xiao, W., Cao, C., Gao, Z., Hu, Z., Liu, S., ... & Lee, X. 2014. Temporal and spatial variations  
598 in radiation and energy balance across a large freshwater lake in China. *Journal of Hydrology*, 511:  
599 811–824.
- 600 Woolway, R. I., Kraemer, B. M., Lenters, J. D., Merchant, C. J., O'Reilly, C. M., & Sharma, S. (2020).  
601 Global lake responses to climate change. *Nature Reviews Earth & Environment*, 1(8), 388–403.  
602 <https://doi.org/10.1038/s43017-020-0067-5>.
- 603 Woolway, R. I., Verburg, P., Lenters, J. D., Merchant, C. J., Hamilton, D. P., Brookes, J., ... & Jones, I.  
604 D. (2018). Geographic and temporal variations in turbulent heat loss from lakes: A global analysis across  
605 45 lakes. *Limnology and Oceanography*, 63(6), 2436–2449.
- 606 Wu, H., Huang, Q., Fu, C., Song, F., Liu, J., & Li, J. (2021). Stable isotope signatures of river and lake  
607 water from Poyang Lake, China: Implications for river-lake interactions. *Journal of Hydrology*, 592,  
608 125619.
- 609 Wu, H., Song, F., Li, J., Zhou, Y., Zhang, J., & Fu, C. (2022). Surface water isoscapes ( $\delta^{18}\text{O}$  and  $\delta^2\text{H}$ )  
610 reveal dual effects of damming and drought on the Yangtze River water cycles. *Journal of Hydrology*,  
611 610, 127847.
- 612 Wurtsbaugh, W. A., Miller, C., Null, S. E., DeRose, R. J., Wilcock, P., Hahnenberger, M., ... & Moore, J.



- 
- 613 (2017). Decline of the world's saline lakes. *Nature Geoscience*, 10(11), 816–821.
- 614 Xiao, M., & Cui, Y. (2021). Source of evaporation for the seasonal precipitation in the Pearl River Delta,  
615 China. *Water Resources Research*, e2020WR028564.
- 616 Yang, K., Hou, J., Wang, J., Lei, Y., Zhu, L., Chen, Y., ... & He, X. (2021). A new finding on the  
617 prevalence of rapid water warming during lake ice melting on the Tibetan Plateau. *Science Bulletin*.
- 618 Yang, K., Wu, H., Qin, J., Lin, C., Tang, W., & Chen, Y. (2014). Recent climate changes over the Tibetan  
619 Plateau and their impacts on energy and water cycle: A review. *Global and Planetary Change*, 112, 79–  
620 91.
- 621 Zhang, Q., & Liu, H. (2014). Seasonal changes in physical processes controlling evaporation over inland  
622 water. *Journal of Geophysical Research: Atmospheres*, 119(16), 9779–979.



---

623 **Figure Legends**

624 **Figure 1. Location of Qinghai Lake (below) and the measurement site of the Chinese Torpedo**  
625 **Qinghai Lake test base (upper).** The insets in the upper picture are photos of the four-way radiometer  
626 and infrared thermometer (left), meteorological variable measurements (middle), and eddy covariance  
627 sensors (right).

628 **Figure 2. Diurnal characteristics of evaporation (E), latent heat flux (LE), sensible heat flux (H),**  
629 **heat storage change (G) and net radiation (Rn) of Qinghai Lake (QHL) during the ice-free (IF)**  
630 **and ice-covered (IC) periods from 2014 to 2018.** The multiday average 30-min data during the IF and  
631 IC in each cycle year are shown here, and the colored shading indicates a 0.5 standard deviation. The  
632 gray area indicates nighttime. The labels 2014/2015, 2015/2016, 2016/2017, 2017/2018 and 2018/2019  
633 indicate the cycle year of the freeze-thaw cycles.

634 **Figure 3. Evaporation (E) rate (a, c, and e) and annual E sum (b, d and f) of Qinghai Lake (QHL)**  
635 **during the cycle year (annual: AN), ice-free (IF) and ice-covered (IC) periods in each cycle year**  
636 **from 2014 to 2018.** a and b show daily data, c and d show daytime data, and e and f show nighttime data.  
637 The whiskers in a, c and e show the 1.5 interquartile range, while the letter associated with the whiskers  
638 indicates statistically significant differences via one-way ANOVA during the different freeze-thaw  
639 periods in each year from 2014 to 2018. The labels 2014/2015, 2015/2016, 2016/2017, 2017/2018, and  
640 2018/2019 indicate the cycle year of freeze-thaw cycling.

641 **Figure 4. Sensitivity coefficient between the daytime and nighttime climatic factors and**  
642 **evaporation (E) rate of Qinghai Lake (QHL) during the ice-free (IF) and ice-covered (IC) periods.**  
643 \*, \*\* and \*\*\* indicate statistical significance at the  $P < 0.1$ ,  $P < 0.05$  and  $P < 0.01$  levels, respectively,  
644 via Student's t tests. Rn,  $\Delta e$ , WS, WD, Pres, Ta-Ts, Tl and ICR indicate the net radiation, vapor pressure  
645 difference, wind speed, wind direction, Pres, the difference between the air and lake surface temperatures,  
646 the average temperature of the lake body from 0 to 300 cm, and ice coverage rate, respectively.

647 **Figure 5. Interannual variability in the simulated evaporation (E) rate (a-c) and annual E sum**  
648 **(d-f) of Qinghai Lake (QHL) in the cycle year (annual: AN), ice-free (IF), and ice-covered (IC)**  
649 **periods from 2003 to 2017.** The blue shading indicates a 0.5 standard deviation, and the red shading



---

650 indicates the 95% confidence interval of the trend line.

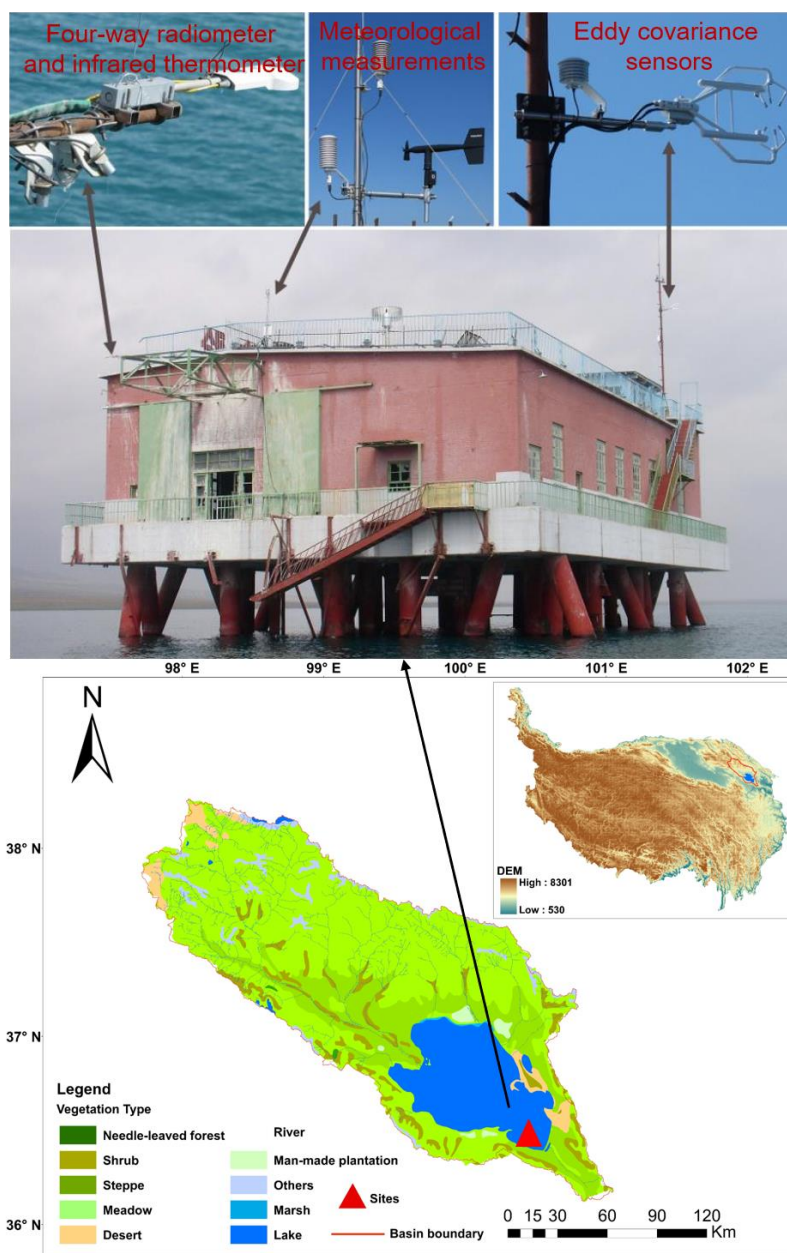
651 **Figure 6. Evaporation (E) and heat storage change (G) in Qinghai Lake (QHL) during the ice-free**  
652 **(IF) and ice-covered (IC) periods.** WS, Pres,  $\Delta e$ ,  $T_a - T_s$ , Rn, and ICR are the wind speed, air pressure,  
653 vapor pressure difference, difference between  $T_a$  and  $T_s$ , net radiation, and ice coverage rate of the lake,  
654 respectively. The red plus sign indicates a positive effect of the variable on E.

655 **Figure 7. The multiyear average contribution of the changes in air temperature ( $T_a$ ), lake surface**  
656 **temperature ( $T_s$ ), downward shortwave radiation ( $R_s$ ), and wind speed (WS) to the simulated**  
657 **evaporation (E) of Qinghai Lake (QHL) in the cycle year (annual: AN), ice-free (IF) and ice-**  
658 **covered (IC) periods from 2003 to 2017.** a shows the multiyear average change in the E rate caused by  
659  $T_a$ ,  $T_s$ ,  $R_s$ , and WS; b shows the multiyear average change in the annual E sum caused by  $T_a$ ,  $T_s$ ,  $R_s$ , and  
660 WS; and c shows the multiyear average change percentage of E caused by  $T_a$ ,  $T_s$ ,  $R_s$ , and WS. The  
661 whiskers indicate a 0.5 standard deviation.



662 **Figures**

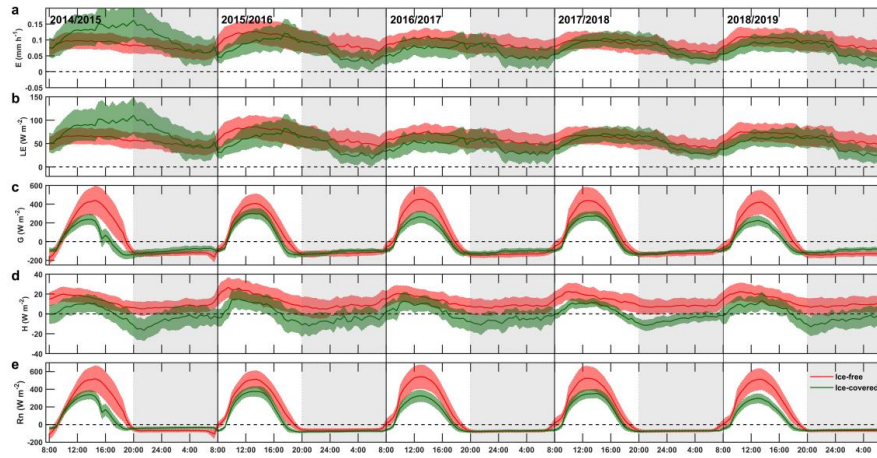
663 **Figure 1.**



664



665 **Figure 2.**



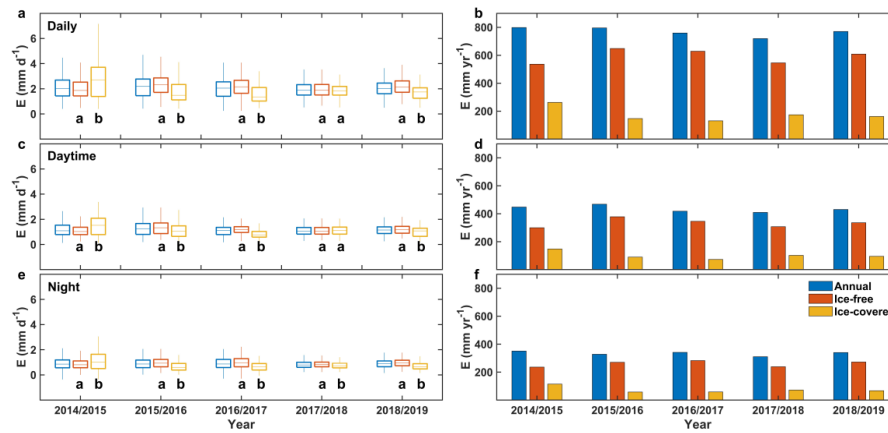
666

667

668



669 **Figure 3.**

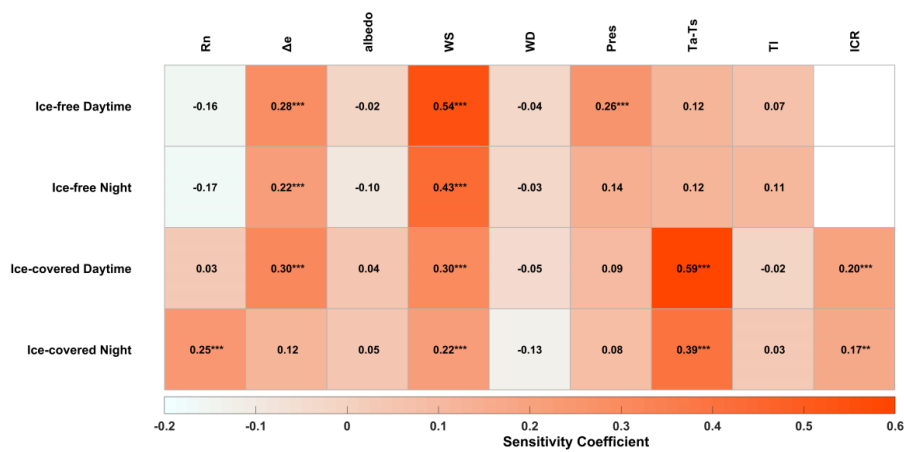


670

671



672 **Figure 4.**

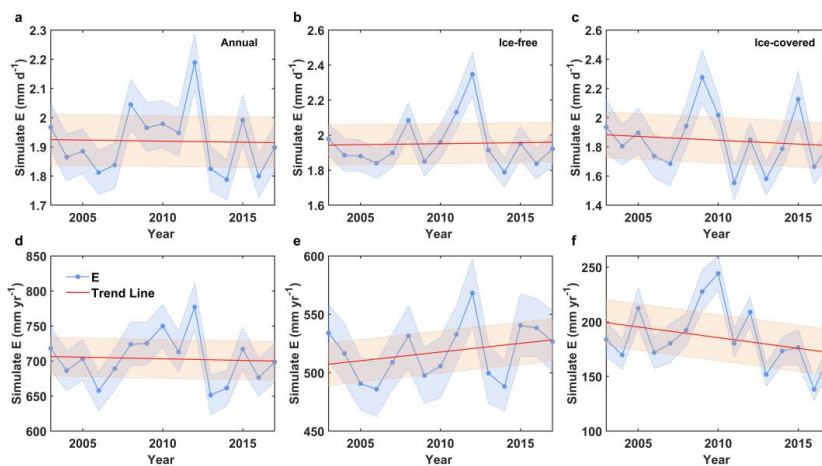


673

674



675 **Figure 5.**

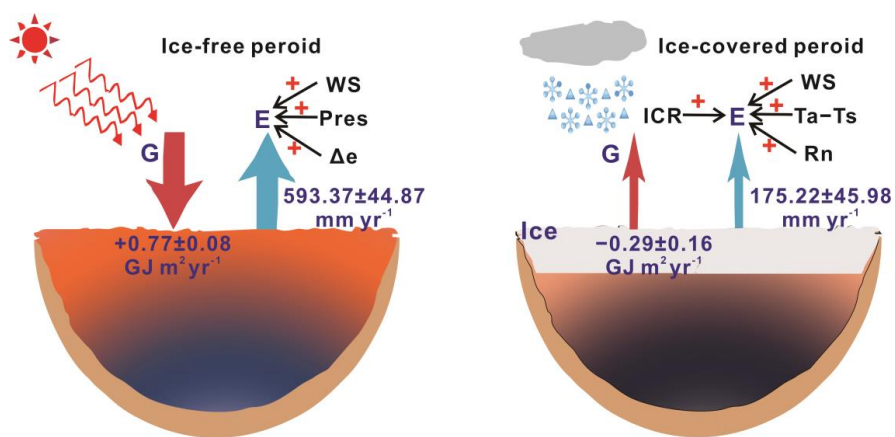


676

677



678 **Figure 6.**

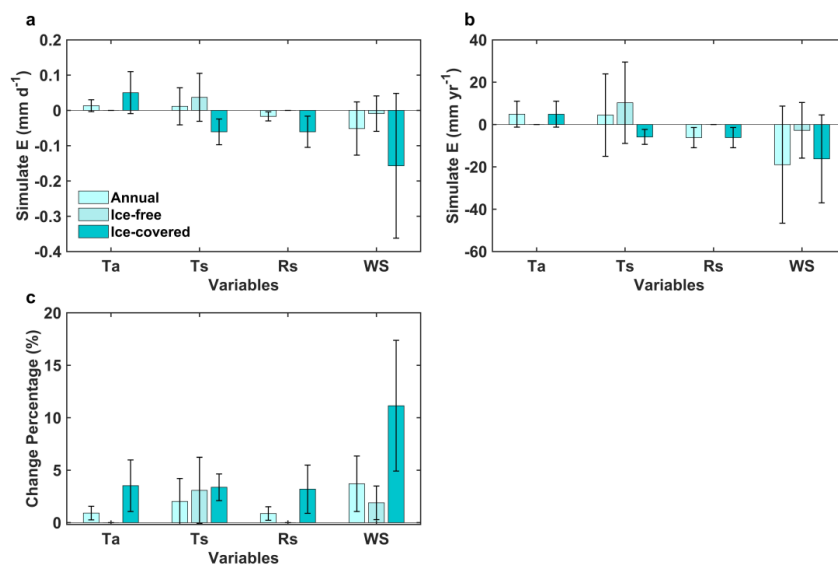


679

680



681 **Figure 7.**



682

683